Int. J. Electrochem. Sci., 12 **(2017)** 797 – 811, doi: 10.20964/2017.01.100

International Journal of
ELECTROCHEMICAL
SCIENCE
www.electrochemsci.org

Surface and Electrochemical Characterization of N-Fe-doped-TiO_2 Nanoparticle Prepared by Hydrothermal and Facile Electro-Deposition Method for Visible Light Driven Pollutant Removal

R. Jothi Ramalingam[1,*], *Prabhakarn Arunachalam*[3],*T. Radhika*[2,*], *K. R. Anju*[2], *K. C. Nimitha*[2],
H A. Al-Lohedan[1]

[1] Surfactants Research Chair, Chemistry Department, College of Science, King Saud University, P.O. 2242, Riyadh 11451, Kingdom of Saudi Arabia.
[2] Centre for Materials for Electronics Technology [C-MET, DietY], Athani, Thrissur-680581, Kerala, India.
[3]Electrochemistry Research Group, Chemistry Department, College of Science, King Saud University, Riyadh, 11451, Saudi Arabia.
[*]E-mail: jothiram@gmail.com, jrajabathar@kus.edu.sa

Received: 7 August 2016 / *Accepted:* 22 September 2016 / *Published:* 12 December 2016

Nitrogen-doped TiO_2 and Fe-N-TiO_2 nanoparticles having rectangular morphology were prepared by a hydrothermal method. A fixed amount N and Fe (III) chlorides was incorporated in a matrix of TiO_2 lattice. The XRD patterns of the as-prepared N- and Fe-doped TiO_2 samples show the presence of only the characteristic peaks of the anatase phase. The formation of the anatase phase in the N-doped TiO_2 photo catalyst was further confirmed by Raman spectroscopy. The particle size of the prepared samples was determined by transmission electron microscopy (TEM) analysis as well as by a particle size analyser. The TEM images revealed that the N-doped TiO_2 nanoparticles possessed a rectangular morphology and had a particle size in the range of 5–10 nm. The average particle size of the Fe-TiO_2nanoparticles was found to be in the range of 2–10 nm. The photo electrochemical and photocatalytic properties of the as-prepared N- TiO_2 and N-Fe-TiO_2 nanoparticles towards the UV and Visible light condition and catalytic degradation of methylene blue (MB) dye were examined under visible light. These N- and Fe-doped TiO_2 nanoparticles are promising materials for the generation of hydrogen fuel through water splitting in the presence of solar light owing to the alteration in their band gaps after heteroatom modification.

Keywords: TiO_2 nanoparticle, methylene blue, electro catalysis, photo catalysis, visible light

1. INTRODUCTION

The development of efficient nanosized photosensitive catalysts has gained immense interest in the field of solar catalysis. Titanium dioxides one of the most promising materials for harvesting light energy for renewable energy applications [1]. Solar energy is abundantly available for most part of the year in India and Saudi Arabia, both of which lie in the tropic and subtropics regions of the equator. Hence, these countries have vast solar potential for revolutionizing green technology by the production of hydrogen. The degradation of hazardous industrial chemicals and dyes using nanoparticle catalysts could provide direct economic benefits to the society and stock holders of renewable energy technology [3]. The photocatalytic activity of nanoparticle catalysts is affected by their physico-chemical properties such as the specific surface area, acid-base sites, and crystalline structure as well as the reaction conditions such as temperature, pH and light intensity. The catalyst preparation methodology significantly affects the final properties of the nanocatalysts. All the above-mentioned factors are responsible for the generation rate of the electron-hole pairs as well as their recombination rate. Many studies have investigated the effect of the structure or particle morphology on the photocatalytic properties of TiO_2 based nanocatalysts and have reported that in contrast to the rutile structure, which displays a radiative recombination process, the anatase structure shows a lower recombination rate [4]. Moreover, the nanoscale size of photo catalysts, which enhances their surface area and the presence of acid sites that aid the adsorption of substrate, are important for improving their catalytic activities. Anatase phase is transform into the rutile phase at temperatures higher than 600^oC when present in the bulk form. An increase in the size of nanoparticles results in the reduction of their surface area. For this reason, the rutile phase, which has a lower surface area, displays a high recombination rate, which in turn, decreases its photocatalytic activity. Despite the fact that the rutile phase shows a poor catalytic activity, nanocatalysts with a heterogeneous structure consists of the anatase and rutile phase show better photocatalytic activities because of the transfer of electrons to the rutile phase to avoid reducing the recombination rate [5–7]. The introduction of heteroatom/transition metal dopants can result in a carrier separation through redox reactions, which then alters the band gap of the photocatalytic system [8]. In order to use the direct sunlight in the photocatalytic processes by doping with transition metal ion dopants such as chromium, iron, and vanadium [9, 10] or heteroatoms like sulphur, nitrogen and carbon has become an alternative catalytic materials and it results in the formation of newly generated energy levels present in the intra gap give rise to the reduction of the associated band gap [11–13]. According to previous reports [14, 15], N doping of anatase TiO_2 having different morphological structures either results in a significant reduction in the band-gap or introduces localize energy level in the gap corresponding to the interstitial or substitutional N atoms in the TiO_2 lattice [16,17]. In the latter case, an Urbach tail is formed in the visible region indicating electronic transition between these localize intragap energy levels. The defects in the TiO_2 lattice like O^- vacancies or interstitial Ti^{3+}, which are either caused because of the nanosize of the particles or also involved in the formation of the new energy levels [17]. It is worth noting that these new levels act as recombination centers or carrier traps during the photocatalytic process [18, 19]. The hydrothermal method is promising for the synthesis of materials with narrow particle size distribution, high purity, and controlled nanostructure morphology. In the present work, N-TiO_2 and Fe-N-TiO_2 nanoparticles were prepared by the hydrothermal method by using known amounts of N and Fe dopants and their morphology was investigated using various physico-chemical techniques. The photocatalytic activity was examined using methylene blue (MB) dye as a model pollutant molecule in an immersion type photo reactor under direct solar-irradiation.

2. EXPERIMENTAL

2.1 Materials Preparation

Titanium butoxide ($Ti(OC_4H_9)_4$, Sigma Aldrich) was hydrolysed using distilled water, and the pH was adjusted to basic values with ammonia solution (Merck). The reaction mixture was then transferred into a Teflon lined autoclave and placed in an oven at 160 ^oC for 6 h. The mixture was then centrifuged and subsequently dried and calcined at 773 K for 3 h to yield TiO_2nanoparticles. To prepare N-and Fe-N-TiO_2, the same procedure was followed with the addition of NH_3 solution (xN:T, x = 0.25, 0.5, and 1.0 molar ratio) and $Fe(NO_3)_3.9H_2O$ (Merck). In order to prepare Fe-N-TiO_2, a solution of Fe $(NO_3)_3.9H_2O$ in water and an appropriate amount Fe with respect to NTiO_2were added together with titanium butoxide along with NH_3 solution and the abovementioned procedure was followed. After 2–3 times of proper washing with distilled water, the products so obtained were dried overnight in an oven. The dried nanoparticle samples were further calcined at 500 ^oC for 2 h for photocatalytic applications.

2.2 Photo electrochemical deposition of Fe and N-TiO_2

TiO_2 (with differing N content) and Fe, N doped TiO_2 film photo anodes were prepared by electrophoretic deposition route on Indium-doped tin oxide substrates. In the present study, 3 mg of Iodine and 15 mg of Fe- or N-TiO_2 powder were dispersed in acetone (15 ml) followed by ultrasonicate in water bath for 5-10 minutes to obtain ordered dispersion of NT powders. The ITO conducting substrate was immersed, parallel to each other with the distance of 1 cm, and then potential of +10 V was applied between them for 4 min *via* biologic electrochemical work station. The photo catalyst particles will be deposited on negative ITO substrates. The prepared photo anodes was then rinsed with deionize water, followed by drying and then calcination at 350 ^oC for 60 min under N_2 atmosphere. The images of electrodeposition (Fe,N)TiO_2 are shown in graphical abstract as well as in Fig. 15a.

2.3 Physico-chemical Characterization

The crystal and phase structures of the synthesized nanomaterials were characterized using powder X-ray diffraction (XRD) (AXS Bruker D5005 X-ray diffractometer), TG-DSC, Raman spectroscopy (DSR Raman microscope), FT-IR spectroscopy, and diffuse reflectance spectroscopy (JASCO UV-Visible spectrophotometer V550 ISV469). The degradation of MB was carried out in an immersion type photoreactorunder visible light irradiation.The degradation kinetics wasmeasured by a UV-Visible spectrophotometer (Perkin Elmer-USA model Lambda 35). The particle size of the as-prepared nanocatalysts was measured using particle size analyser (Nanoplus-1) providing a resolution in the range of 0.1 nm to 10 µm. The morphology of the doped TiO_2 nanoparticles was analyzed by transmission electron microscope (TEM) (JEOL-JEM-2100F) operating at an acceleration voltage of 200 kV. High resolution transmission electron microscopy (JSM-T 220A, JEOL) was used to study the surface morphologies of the as-prepared nanomaterials with at acceleration voltage of 20 kV.

2.4. Photo electrochemical characterization

All Electrochemical measurements were conducted in a H type electrode cell that was composed of an electrodeposited TiO_2 based photo anodes as a working electrode, platinum served as a counter electrode and a saturated Calomel electrode (3M KCl) electrode as a reference electrode. The electrolyte was a 1 M Na_2SO_4(aq) solution at pH=13 adjusted by adding drops of 1.0 M KOH. CV and EIS measurements were performed on Biologic electrochemical analyzer workstation. The test potential ranged from open circuit potential to 2.0 V and the frequency ranged from 100 kHz to 1 Hz. The light source was acquired from the solar simulator (Asahi, MAX303 300 W).

The solar energy harvesting abilities of the prepared N-TiO_2 and Fe-N-TiO_2nanoparticleswere analysed by the photosensitive degradation/decolouration of MB under direct irradiation by visible light. MB is an important organic dye used in the chemical industry and was used as a model pollutant in the present study. Small aliquots were withdrawn at known intervals and absorbance was recorded using UV-Visible spectroscope (Perkin Elmer-USA model Lambda 35). Experiments were also conducted in dark.

3. RESULTS AND DISCUSSION

3.1 Powder X-ray diffraction characterization

The powder XRD patterns for N-TiO_2 samples with different amounts of nitrogen prepared by the hydrothermal method after calcination at 500 ^oC are shown in Fig 1. The XRD patterns showed well resolved characteristic peaks of anatase phase ((101), (004), (200), (105), (204), (211), and (215)). Thus, N-TiO_2 synthesized using the hydrothermal method under appropriate addition of nitrogen consisted purely of the anatase phase.

The crystallite size was calculated using Scherrer equation and was found to be ~25 nm. The lattice parameters are in good agreement with the reported JCPDS values (JCPDS 04-002-2678, JCPDS21-1272), which confirms the presence of the anatase phase in the hydrothermally prepared N-$TiO_{2.}$ Figure 1 shows the powder X-ray diffraction patterns of N-$TiO_2$with different xN:Ti (x= 0.25,0.50, 1.0N) ratios.

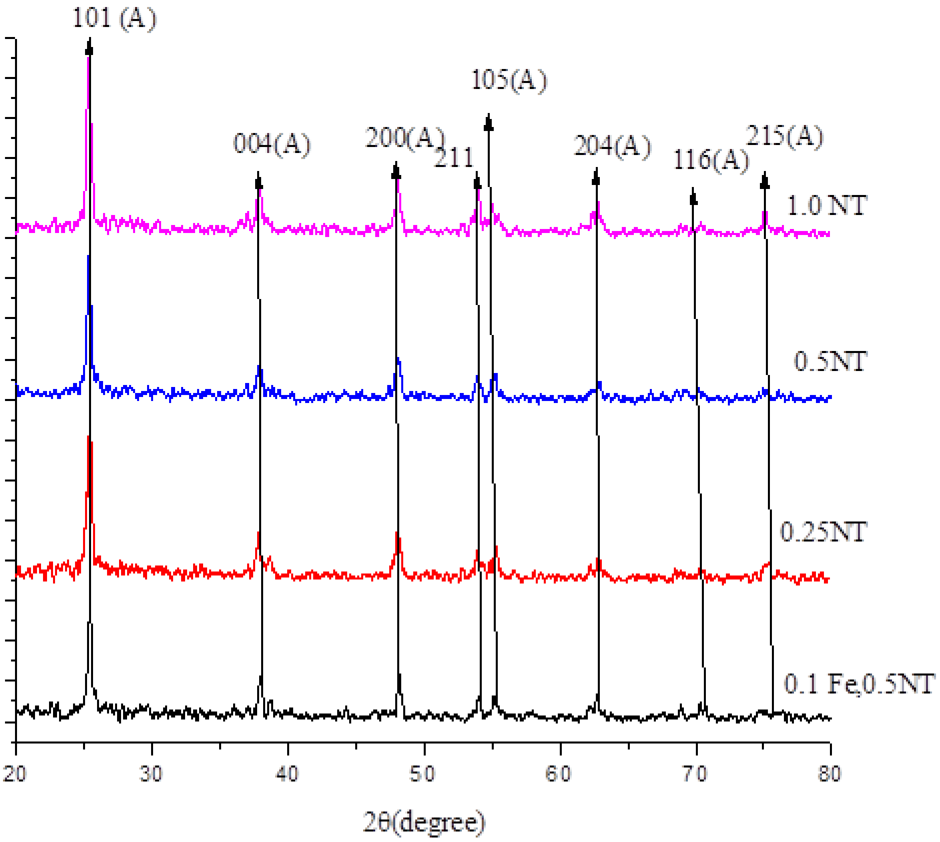

Figure 1. XRD patterns of N- and Fe-doped TiO_2 samples containing different amounts of N and Fe dopants.

The peak corresponding to the (101) plane of the anatase phase was the most intense. The crystallite size of all the three samples with different N:Ti ratios were calculated and were found to be 25 (0.25N:1Ti), 24.3 (0.5N:1Ti), 25.9 nm (1N:1Ti). It was found that the crystallite size increased with an increase in the N:Ti ratio. The lattice parameters a, b, and c were consistent with those of the anatase phase. The XRD patterns of the N-doped TiO_2 nanoparticle catalysts (Figure 1) showed that the anatase phase was dominant in the catalysts [20]. The Fe-N-TiO_2 sample was readily indexed to the diffraction peak of the anatase phase (JCPDS 04-002-2678), and showed the presence of an intense peak corresponding to the (101) plane of the anatase phase. The XRD peaks of Fe-N-TiO_2 shifted slightly to the right of the X axis as compared to those of N-TiO_2. In the case of 0.02 Fe-N-TiO_2, the (101) peak was less crystalline. The major peaks observed corresponded to the (101), (004), (105), (211), (116), and (215) planes of the anatase phase. For 0.01, 0.05, and 0.1 Fe-N-TiO_2 samples, the crystallite sizes were found to be 32.4, 29.1, and 35 nm, respectively. This shows that as the co-doping concentration of Fe increased, the crystallite size of the samples also increased. The lattice parameters matched well with the reported standard values [20]. The crystallite size and lattice parameters obtained from the XRD results for all the prepared samples. The XRD patterns of the N-TiO_2 and Fe-NTiO_2 samples showed that only crystalline anatase TiO_2 phase was present in all the samples [5]. For

N-TiO_2, the crystallite size was found to be within the range 22–25 nm. However, for Fe-N-TiO_2, the crystallite size increased up to 32nm.

Table 1. Band gap energy and λmax of the doped TiO_2 photo catalysts

Sl. No:	Material prepared	λ_{max}	Band gap energy (eV)	
			Calculated	Tauc plot
1.	0.25N-TiO_2	473	2.62	2.64
2.	0.5N-TiO_2	526	2.35	2.20
3.	1.0N-TiO_2	590	2.09	2.01
4.	0.1Fe1.0N-TiO_2	602	2.05	1.99

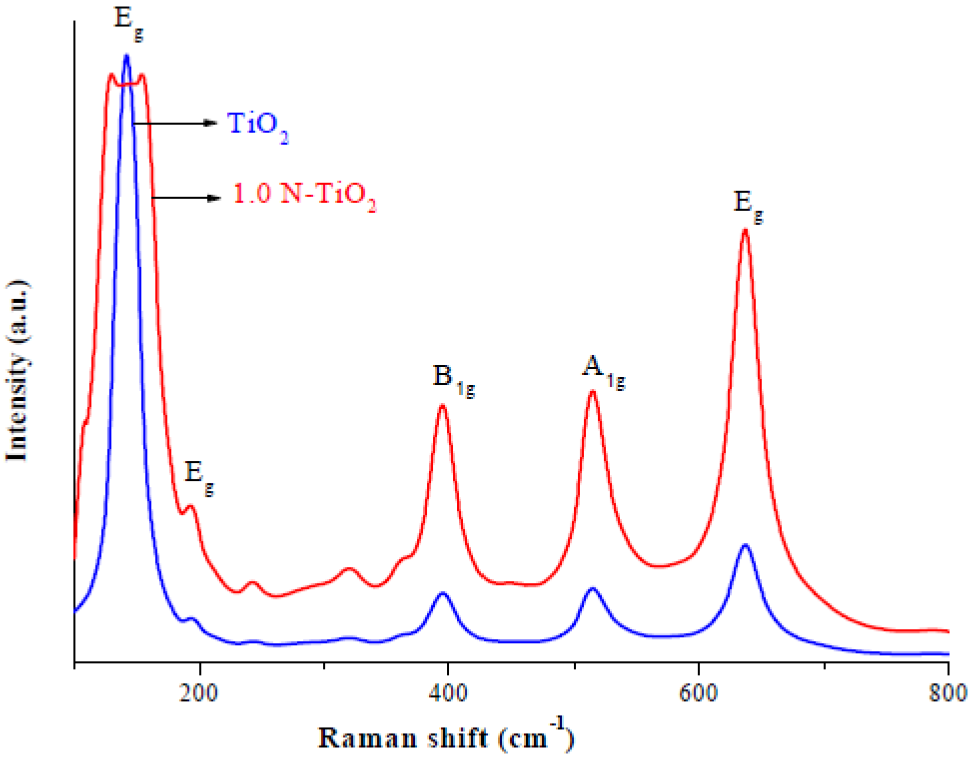

Figure 2. Raman spectra of TiO_2 and N-TiO_2.

Figure 2 shows the Raman spectra of TiO_2 and N-TiO_2. The characteristic Raman active modes for anatase TiO_2 (Eg and B1g) were observed. The Raman spectroscopy results confirmed the presence of the anatase phase in TiO_2 and N-TiO_2 and were in agreement with the XRD results [21]. The FT-IR spectra and TG-DSC analysis of the samples confirmed that organic material present in the samples was completely removed after calcination to form an anatase TiO_2 lattice [22]. Even though the trend for the variation of crystallite size was not very clear, the crystallite size decreased when the content of Fe ions increased from 0.1 to 1.0 mol% [23]. According to the factor group analysis, anatase TiO_2 has 6 Raman active modes of vibrations: one A_{1g}, two B_{1g}, and three $E_g$modes. The three E_g modes are centred on 145,197, and 639 cm^{-1}, the two B_{1g} modes are centred at 399 and 519 cm^{-1} and the one A_{1g} mode is centred at 513 cm^{-1}. The bands at 144 cm^{-1} (Eg), 199 cm^{-1}(Eg), 398 cm^{-1} (B1g), and the doublet band at 522 (A1g and B1g modes) and 633 cm^{1} (Eg) confirmed the presence of anatase TiO_2 in the synthesized N-TiO_2 TiO_2 materials [24]. The Raman spectrum of the TiO_2 sample calcined at 773 K is shown in Fig. 2. As shown in Fig. 2, the Raman spectrum of TiO_2 prepared by the hydrothermal method exhibited bands at ~144, 191, 393, 513, and 636 cm^{-1}. The band at 146 $cm^{-1}$was the most intense. All the modes observed for the prepared TiO_2 corresponded to the anatase phase. Thus, the Raman spectroscopy results confirmed that only the anatase phase was present in the prepared TiO_2 as evidenced by XRD. However, the observed peaks in the Raman spectrum showed red shift. This shift may be attributed to the change in the oxygen deficiency at the TiO_2 surface. This may be due to the effect of N doping onto the TiO_2 lattice with surface oxygen deficiency, which facilitates the formation of TiO_2 nanoparticles with low crystallinity.

3.2 TG-DSC and Ft-IR characterization

The TG-DSC profiles for the as-prepared TiO_2 and Fe-TiO_2 are shown Fig.3. The analysis was carried out at temperatures ranging from room temperature to 1000 °C. An endothermic peak observed at ~100 °C represents the unbound water being removed from the TiO_2 surface (Fig. 3A). A minor exothermic peak at 400°C indicates the crystallisation of amorphous TiO_2 to anatase structure. At temperatures above 500°C, the change in the weight of the samples was very less, which confirms the complete formation of anatase TiO_2 in this region. Thus, 500°C was used as the calcination temperature for the preparation of these materials.

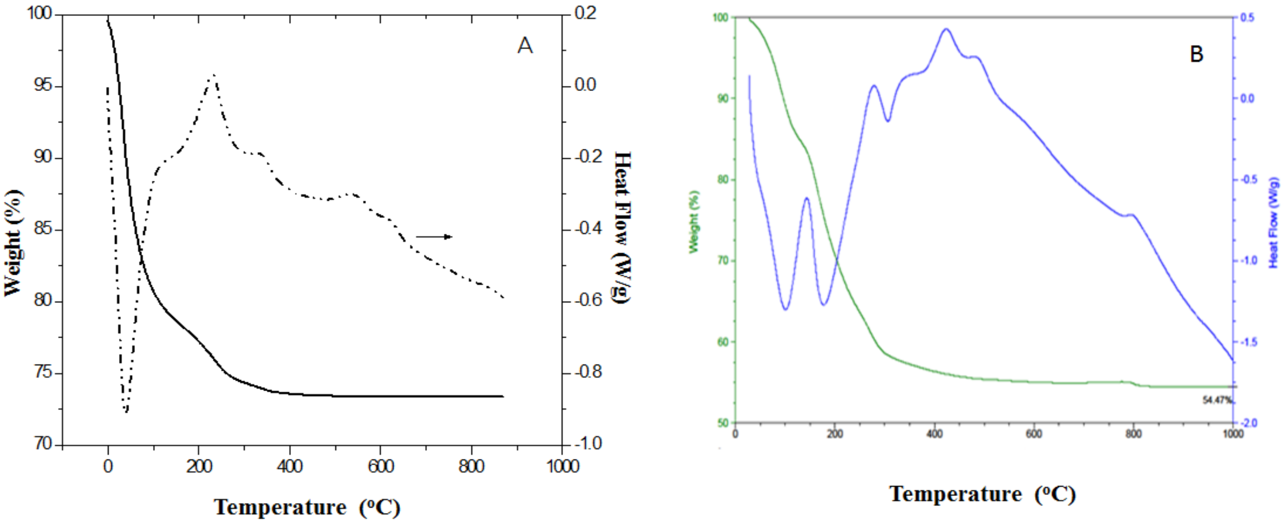

Figure 3. TG- DSC of (a) pure TiO_2 and (b) 0.1N-TiO_2.

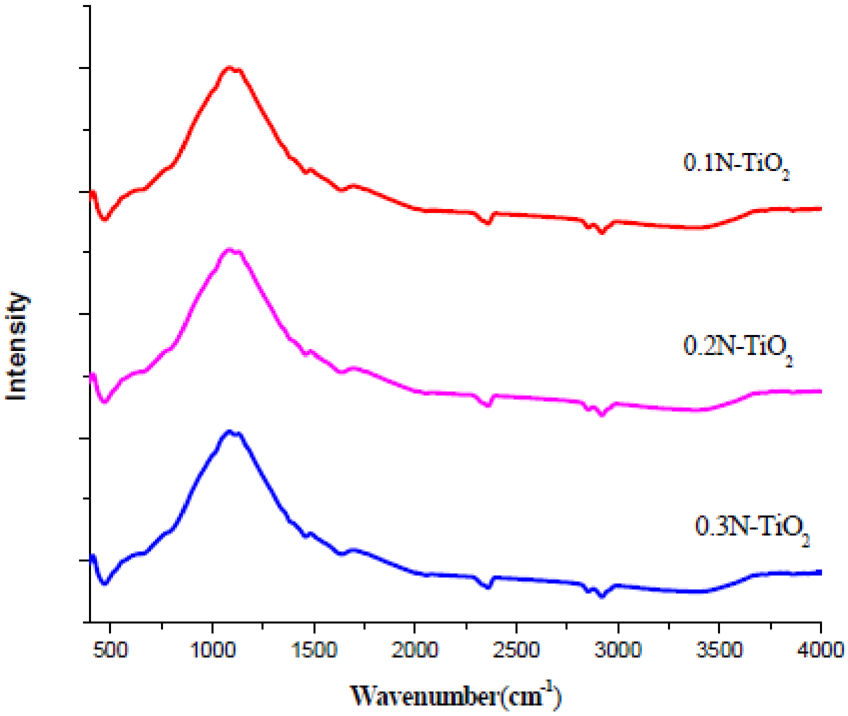

Figure 4. FT-IR spectra of N-TiO_2 samples containing different amounts of N doping in TiO_2.

Figure 3B shows the TG-DSC profile of N-TiO_2. The profile shows the presence of two weak endothermic peaks (80 and 166°C) and one strong exothermic peak (274°C), indicating more weight loss around these temperatures. The weight loss at these temperatures can be attributed to the evaporation of the solvent used and the N precursor and its derivatives. An exothermic peak observed in the range 374–400°C corresponds to the formation of crystalline anatase phase. The thermo gravimetric results also show the removal of the unreacted N precursor at 500°C. From the TG profiles, it is clear that the weight change after 500°C was not significant. However, the observed DSC pattern indicates the transformation of anatase TiO_2 to rutile structure as the temperature increased to 800°C.

The FT-IR spectrum of the hydrothermally prepared TiO_2 (calcined at 500°C) over the range 400–5000 cm^{-1} is shown in Fig. 4. The FT-IR spectrum of TiO_2 shows a band at ~469 cm^{-1}, which can be attributed the Ti-O stretching vibrations. The presence of the band at ~1640 cm^{-1} corresponds to the characteristic bending vibration of the adsorbed water molecules. Furthermore, the bands in the range of 3500–2800 cm^{-1} are attributable to the stretching vibrations of -OH groups. It has been reported that the surface –OH groups, which are quite polar give rise to strong IR bands in the range of 3000–4000 cm^{-1} and 1600–1700 cm^{-1}. The band at 2363 cm^{-1} can be assigned to the vibration of CO_2 from the environment. The absence of the characteristic FT-IR peaks of –OR groups (1100– 1000 cm^{-1}) confirms that the titanium alkoxides were completely hydrolyzed to form TiO_2 nanoparticles during the calcination. FT-IR spectra of N-TiO_2 also indicate Ti-O vibration at 469 cm^{-1}. An additional peak, which is generally observed at ~508 $cm^{-1}$and corresponds to the O-Ti-N and N-Ti-N bond vibrations was absent in the prepared catalysts [25]. This suggests that there was no Ti-N bond formation, supporting the idea of interstitial doping of N into the TiO_2 lattice during the hydrothermal synthesis using NH_3 as a nitrogen precursor. All the other peaks were similar to those obtained for TiO_2.

3.3 Structure and textural characterization of (Fe,N)-TiO_2

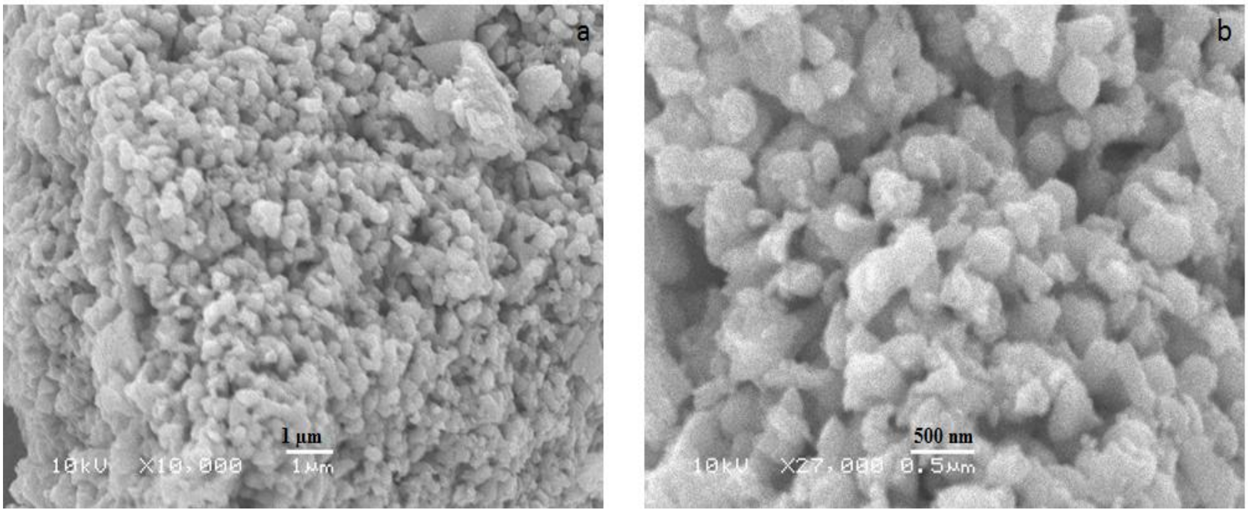

Figure 5. SEM micrographs of 0.1Fe-0.5N-TiO2.

Figure 5 shows the SEM micrographs of the Fe-N-TiO_2 nanoparticles with fine-particle morphology and similar and ordered shape observed below 100 nm. The morphology of the N- and Fe-doped TiO_2 nanoparticles was studied by TEM and SEM analyses. Figures 6 and 7 show the TEM-EDX results of TiO_2 and N-TiO_2. The preparation methodology adopted in the present study, yielded N-TiO_2 nanoparticles having rectangular or square-shaped morphology. The size of the particles was found to be in the range of 5–10 nm. The low particle size provided the active surface sites for absorbing species and altered the inner energy levels of the TiO_2 band structure.

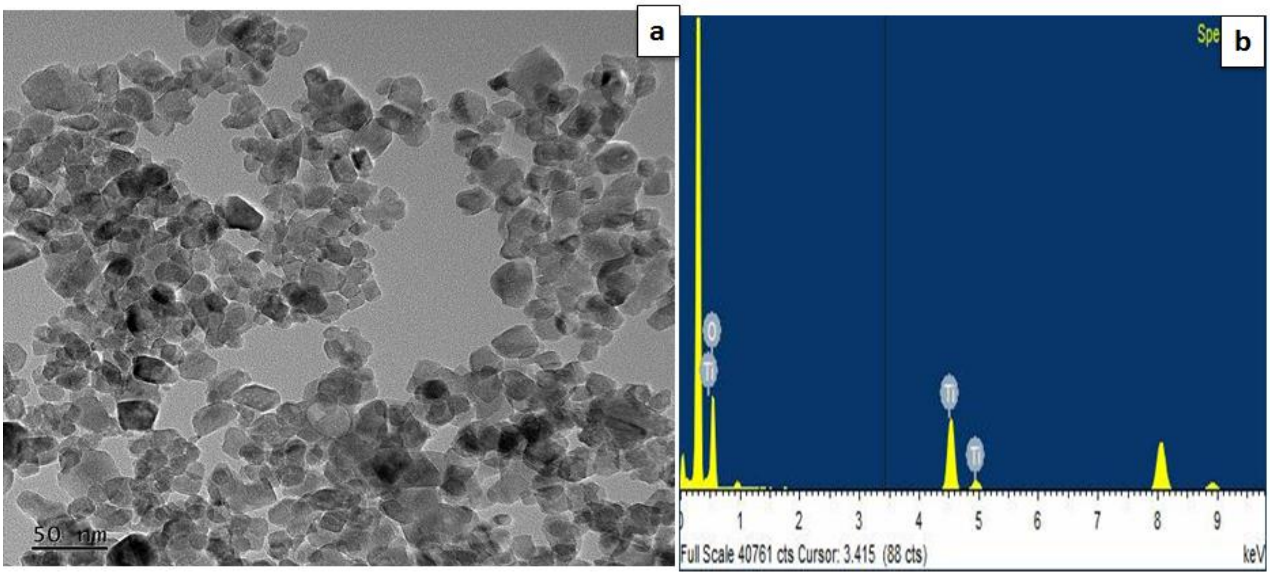

Figure 6. TEM images and EDX spectra of 0.5 N-TiO2.

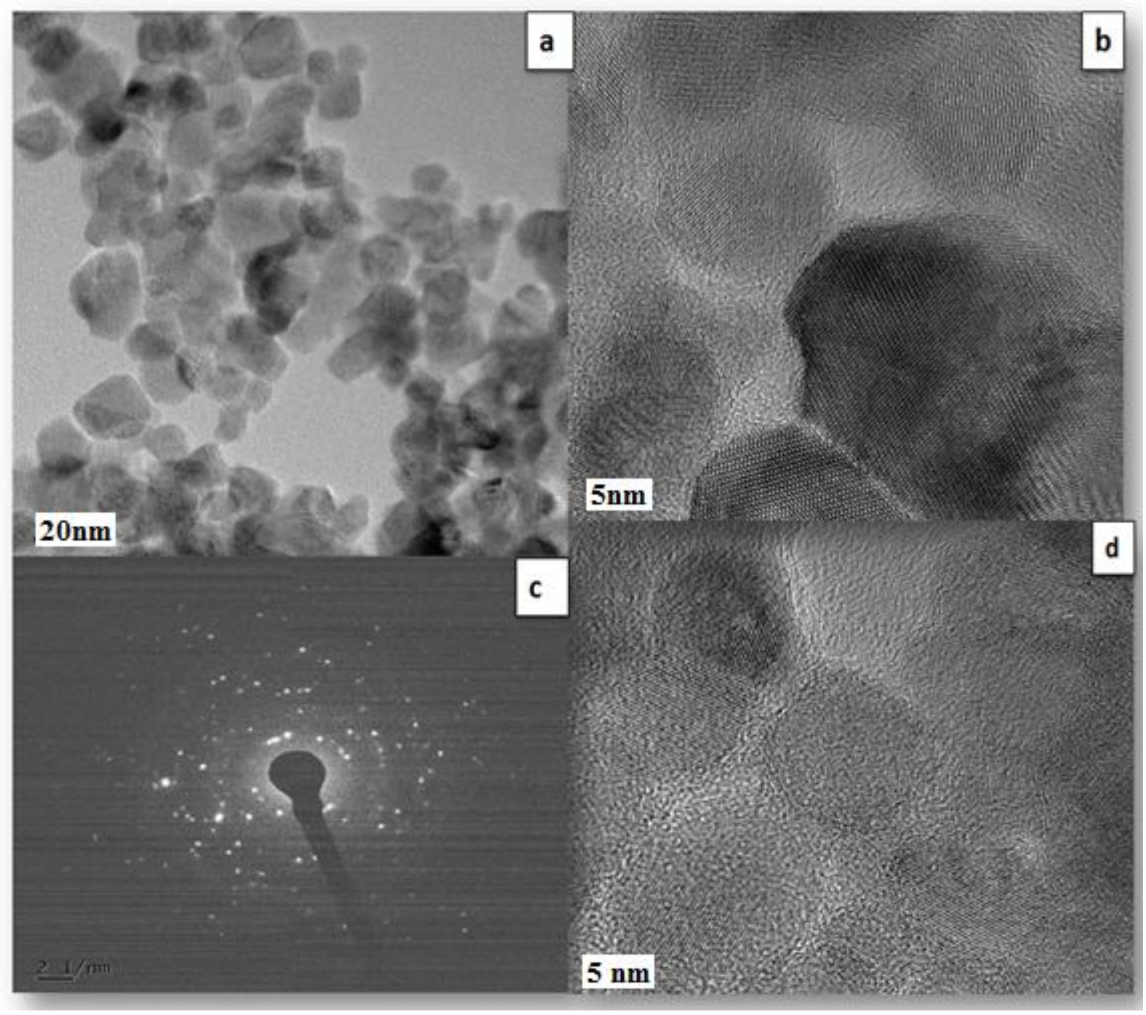

Figure 7. TEM images and electron diffraction pattern of 0.1Fe-0.5N-TiO2.

Light scattering particle size analysis further confirmed that the average particle size distribution for the Fe-N-TiO_2 was below 5 nm.

3.4 Photo electrochemical characterization of deposited (Fe,N)-TiO_2 catalysts

Figure 8a shows the photo electrochemical (PEC) properties of (Fe,N) doped TiO_2 in order to examine and compare the photo electrochemical behavior of (Fe,N)TiO_2 photoanodes, shows LSV (linear sweep voltammetry) at 50 mV s^{-1} for N doped TiO_2 photo anodes in alkaline solutions (pH 13, 1 M Na_2SO_4) under UV light illumination. The enhanced activity with a photocurrent of 0.25 mA/cm^2 at 1 V vs RHE was observed for the NT2 (0.5N:1Ti) photo anode with N content. To further enhance the PEC performance of the optimized NT1 photo anodes, we deposited a (Fe,N) cocatalyst layer by insitu photo deposition method to support the kinetics of the O_2 evolution reaction. In order to observe the effect of (Fe,N) cocatalyst on the photocurrent generation of TiO_2 photo anodes, LSV analysis were performed under Ultra-violet and visible light photons. The obtained results are shown in Fig. 8b and 8c, respectively. These results validates that the photocurrent enhancement observed after modification with (Fe,N) on TiO_2 substrates and iron doping act as a hole and electron trap to inhibit the recombination of the photogenerated electrons and holes. Moreover, Fe doping leads to new states close to the conduction band which results in the enhancement in the photocurrent and the results are consistent with earlier reported literature [26-27]. The (Fe,N) TiO_2 photoandoes showed the highest photo electrochemical performance both in UV and Visible light photons. It can be illustrated that the radius of Fe^{3+} is alike to that of Ti^{4+}, the replacement of iron in the matrix is a stress-free process. When iron ions replace the titanium ions, the formation of defect sites acts as a long-lasting space charge region, whose electric power enhances the separating efficiency of carriers (electron-hole) and leads to the charge-transfer appearance. Moreover, the carrier (election or hole) trapping can diminish the recombination rate and improves their lifetimes, thus enhancing the photo electrochemical performances [26,27]. These PEC features exposed that the (Fe,N) TiO_2 photo electrodes, photocurrent at UV/Visible light photons was comparatively improved after doping, suggests the (Fe,N) doped TiO_2 had enhances the surface redox activity effectively. The charge carrier mobility and band positions of the semiconductor are very essential to recognize the photo electrochemical or photo catalytic reactivity.

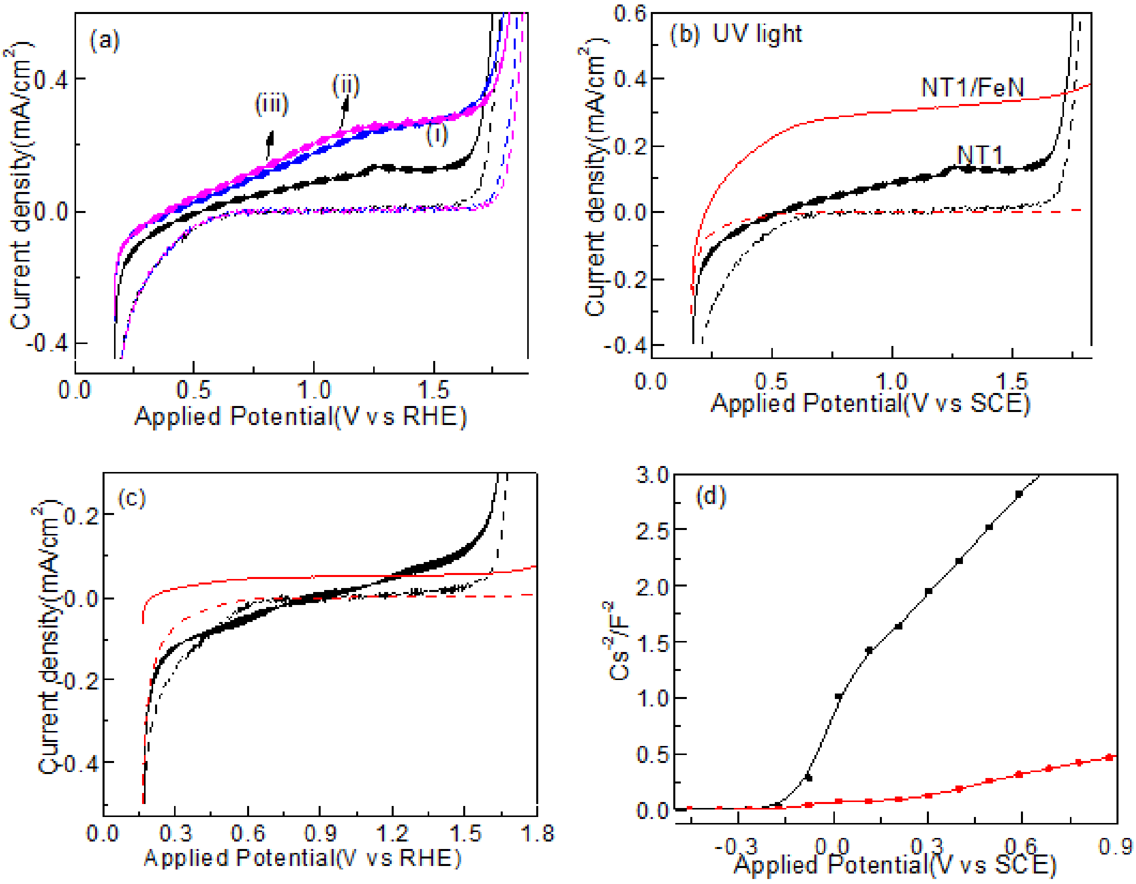

Figure 8. (a) Linear sweep voltammogram (LSV) at 50 mVs^{-1} in 1.0 M $N_{a2}SO4$ at pH 13 for photocurrent response for various kinds of TiO_2 based photo anodes loaded on ITO, (i) N-TiO_2(N: Ti = 1 : 1), (ii) N-TiO_2(N: Ti = 0.5 : 1), (iii) N-TiO_2(N: Ti = 0.25 : 1), (b) plot for photocurrent measured at 2.2 V vs. RHE and amount of N or Fe loaded TiO_2 deposited by electrophoretic route on ITO, (c) photocurrent measure under visible light irradiation on N-TiO_2 and (Fe,N)TiO_2 (d) Mott-scotty curve of N-TiO_2 and (Fe,N)-TiO_2.

Herein, Mott-Schotkky method are applied to understand the activity of (Fe,N)/TiO_2 and TiO_2 films. The Mott Scotty investigation were studied in 1 M phosphate solution (pH =13) at frequency of 100 Hz in dark condition. As shown in Fig.8d, the intercept on the potential of NT1 shows a flat band potential (E_{FB}) is obtained at –0.13V (vs RHE at pH = 13). Whereas, the intercept of the potential axis of (Fe,N) doped TiO_2 displays an E_{FB} is obtained at –0.24 V (vs RHE at pH = 13). The calculated donor density of NT1 and (Fe,N) NT was found to be 2.35×10^{21} cm^{-3} and 56×10^{21} cm^{-3} respectively. It should be noted that the Fe doping results in a notable enhancement of carrier density in (Fe, N) NT photoanodes. Obviously, the increase in carrier and electron concentration in the conduction band, results in Fermi level energy moving close to the CB edge, which enhance the charge separation activity at the NT/electrolyte interface by increasing the degree of band bending at the NT surface [28]. Ostensibly, (Fe,N) doped photoanodes has a more positive flat band potential than undoped electrodes. Noticeably, (Fe,N) was effective way to amend the PEC conducting property of TiO_2 photo electrodes by increasing its donor density and the results are consistent with earlier reports of Fe doped TiO_2 materials [29].

3.5Visible light driven photo catalytic activity

Figure 9 & 10 shows the combined results of the enhanced activity of the photo catalysts like the N-doped TiO_2 NPs and Fe-N-doped TiO_2 NPS for effective or complete discoloration of MB over duration of 6 h under direct visible light irradiation. Figure 9 shows the visible light assisted photocatalytic degradation of MB analyzed at the surface of Nitrogen and Fe (III) doped N-TiO_2. Increasing the nitrongen content and iron doping on TiO_2 increased the methylene blue degradation. The possible mechanism of the Iron doped TiO_2 photo catalysis is as follows; Iron(III) ions in TiO_2 can play as hole and electron traps towards in the formation of Iron(II) and Iron(IV) ions, which are less stable as compared to Iron(III) ions. Hence, the above phenomena leads to the generation of $OH^{\cdot}$ radical and O_2 anion. Therefore, iron concentration is higher, the Iron (III) ions could play as recombination center of the charge carriers, *via* reducing the photo-catalytic activity. Therefore, the above formed highly oxidizing species further oxidize the MB and form intermediates to finally end up in complete mineralization with the release of small molecules. The prepared photo catalysts are showing good reproducible activity. After each reaction, the used catalyst was washed well and dried in oven followed by calcination at 500^{o} C for the next run for the same reaction. The recycled Fe and N-doped TiO_2 nanoparticles showed promising catalytic activity towards the photocatalytic degradation of pollutants. Figures 10A and 10B show the kinetics of dye degradation (such as C/Co and –LnC/Co of MB versus irradiation time) using 0.5N-TiO_2 and 0.1Fe-0.5N-TiO_2, respectively. As it is clear from these figures, the dye degradation obeys a linear pattern in this coordinate with good precision in the both cases. This means that the dye degradation followed pseudo-first order kinetics, which was similar for both the photo catalysts and results similar to the reported kinetic study on methylene blue degradation [30].

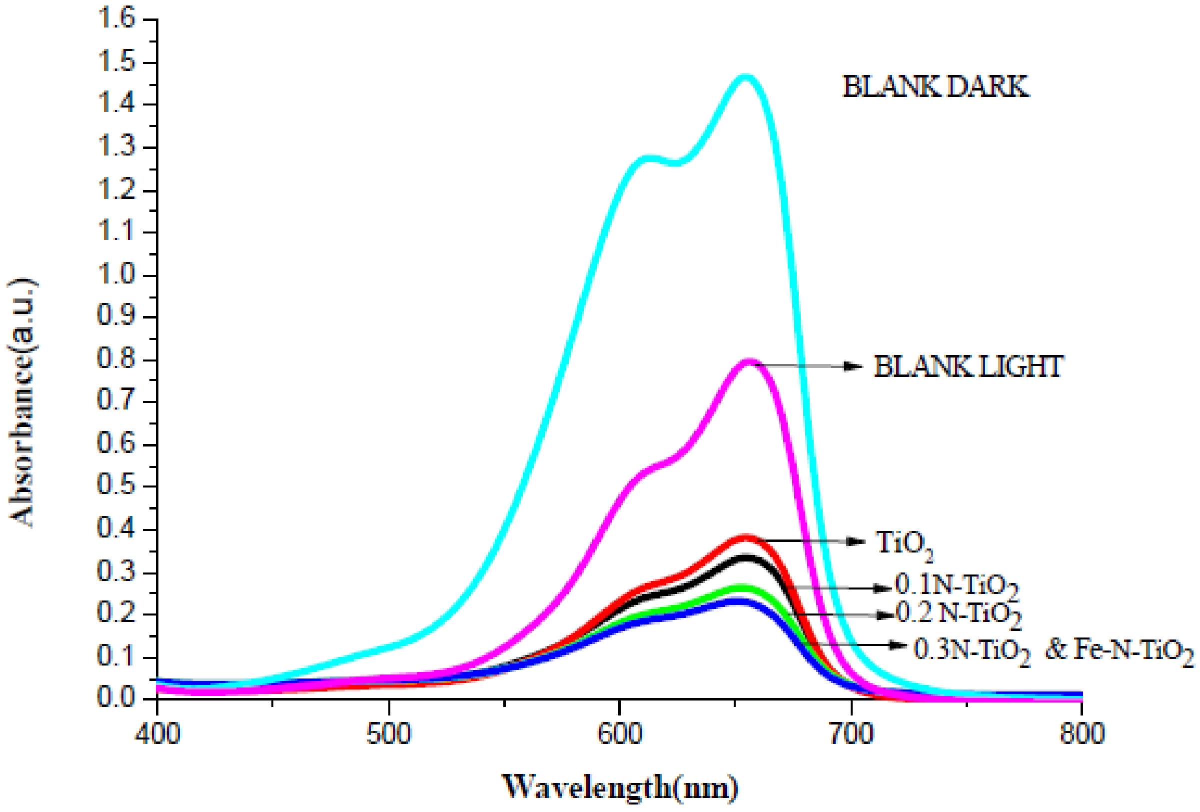

Figure 9. Degradation of MB using N-and Fe-doped TiO2 samples containing different amounts of N and Fe dopants.

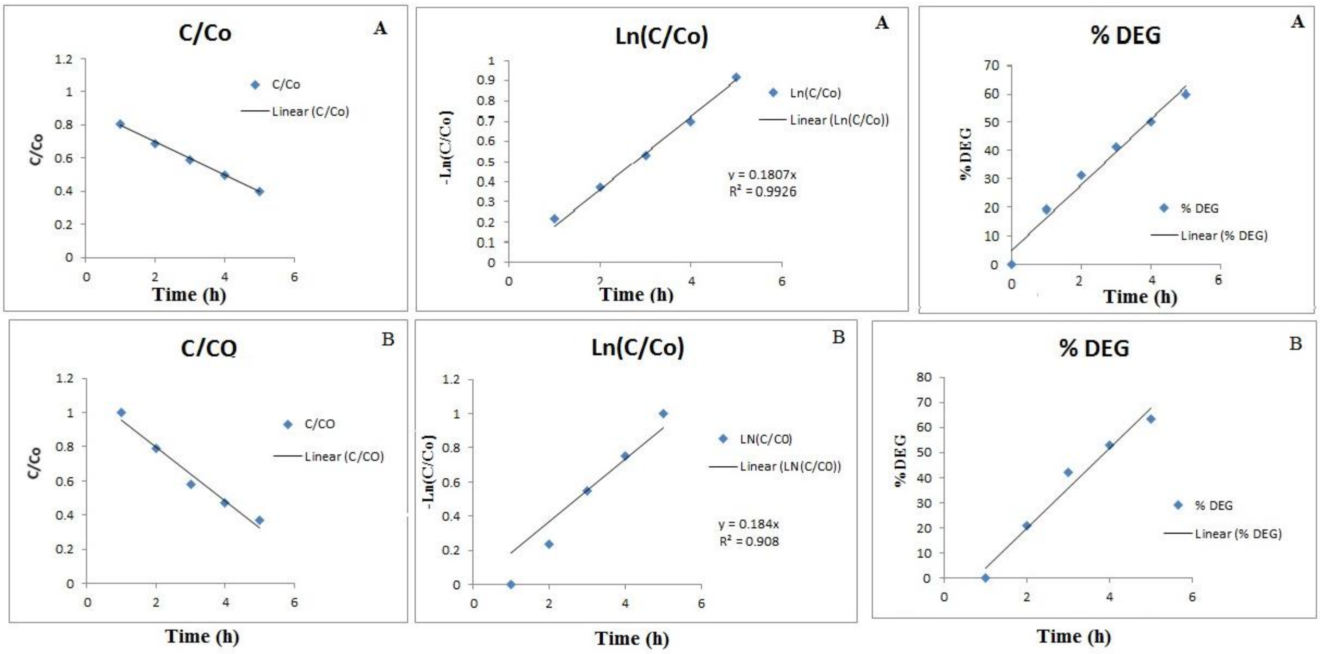

Figure 10. Kinetics of MB degradation using (A) 0.5 N-TiO2 (B) 0.1Fe-0.5N-TiO2.

4. CONCLUSIONS

N- and Fe-doped TiO_2 nanoparticle was synthesized by a one-step template-free hydrothermal method and electro deposition technique. The powder XRD patterns of all the catalysts showed the presence of the crystalline anatase TiO_2 phase with a crystallite size in the range of 20–25 nm for the N-doped TiO_2 nanoparticles. The average particle size for the Fe-N-TiO_2 samples was found to be 12 nm. In the case of the Fe-N-TiO_2photocatalyst, very fine rectangle-shaped nanoparticles were formed. The Raman spectra showed the presence of active modes corresponding to the anatase TiO_2 phase, thus confirming the XRD results. The enhanced activity with a photocurrent of 0.25 mA/cm^2 at 1 V vs RHE was obtained for the NT2 (0.5N:1Ti) photo anode and Fe,N-doped TiO_2 catalysts shows the best result for photo electrochemical and visible light driven catalysis. The synthesized doped TiO_2 nanoparticles are expected to provide promising activity for water splitting reactions for hydrogen production.

ACKNOWLEDGEMENTS
This project was financially supported by King Saud University, Vice Deanship of Scientific Research, Research Chairs.

References

1. O. Ola and M.M. Maroto-Valer,*J Photochem. Photobio. C: Photochemistry Reviews,* 24 (2015) 16.
2. S. Goyal, A. Chodha, D. Singla, A. Singh, *Gyancity Journal of Engineering and Technology,* 2 (2016) 9.
3. C. Burda, Y. Lou, X. Chen, A.C. S. Samia , J. Stout and J. L. Gole *Nano Letters,* 8 (2003)1049.
4. H.S. Jung and H. Kim, *Electron. Mater. Lett.,*5 (2009)73.
5. R.I. Bickley, T. Gonzalez-Carreno, J.S. Lees, L. Palmisano and R.J.D. Tilley, *J. Solid. State Chem.,*92 (1991)178.
6. O.M. Ilinich, E.N. Gribov, P.AN. Simonov, *Catal. Today, 82* (2003)49.
7. R.R. Bacsa and J. Kiwi, *Appl. Catal.B:Environ.,* 16 (1998)19.
8. S. Liu and Y. Chen,*Catal. Commun.,* 10 (2009)894.
9. Y. Liu, J.H. Wei, R. Xiong, C.X. Pan and J. Shi, *Appl. Surf. Sci., 257* (2011) 8121.
10. B. Liu, X. Wang, G. Cai, L. Wen, Y. Song and X. Zhao, *J. Hazard. Mater.,* 169 (2009)1112.
11. D. Cheng, Z. Jiang, J. Geng, Q. Wang and D. Yang, *Ind.Eng.Chem.Res., 46 (*2007) 2741.
12. L. Szatmáry, S. Bakardjieva, J. Subrt,ˇ P. Bezdicka,ˇ J. Jirkovsky,´ Z. Bastl, V. Brezová and M. Korenko, *Catal. Today*, 161 (2011) 23.
13. G. Zhang, Y.C. Zhang, M. Nadagouda, C. Han, K. O'Shea, S.M. El-Sheikh,A.A. Ismail and D.D. Dionysiou, *Appl. Catal. B:Environ.*, 144 (2014) 614.
14. X. Chen and S.S. Mao, *Chem. Rev.,* 107 (2007) 2891.
15. C. Di Valentin, E. Finazzi, G. Pacchioni, A. Selloni, S. Livraghi, M.C. Paganini and E. Giamello, *Chem. Phys.*, 339 (2007) 44.
16. E. Finazzi, C. Di Valentin, A. Selloni and G. Pacchioni, *J. Phys. Chem. C*, 111 (2007) 9275.
17. F. Dong, W. Zhao, Z. Wu and S. Guo, *J. Hazard.Mater.,* 162 (2009) 763.
18. G. Colón, M.C. Hidalgo, G. Munuera, I. Ferino, M.G. Cutrufello and J.A. Navío, *Appl. Catal. B: Environ.,*63(2006) 45.
19. R. Jothiramalinga, M.K. Wang, *Journal of Hazardous Materials*, 147 (2007)562.
20. D.P. Macwan, P. Dave and S. Chaturvedi, *J. Mater.Sci.,*46 (2011) 3669.
21. Y. Z. Yu-Chang Liu, Y. F. Lu and J. C. Chung, *Inter. J. Chem. Eng. Appl.,* 3 (2014) 234.

22. I. Ganesh, P. P. Kumar, A. K. Gupta, P. S. C. Sekhar, K. Radha, G. Padmanabham andG. Sundararajan, *Proce. Appl. Ceram.*, 1 (2012) 21.
23. J.A. Wang, R. Limas-Ballesteros, T. López, A. Moreno, R. Gómez, O. Novaro and X. Bokhimi, *J. Phys. Chem. B*, 105 (2011) 9692.
24. A. Arias, J. C. Caicedo, L. Ipaz, W. Aperador, L. TiradoMejía, G. Zambrano and M.E. Gomez, Rev.*Latinoamericana de Metal. y Mater.,* S14 (2009) 1479.
25. K. Zhang, X. Wang, X. Guo, T.He and Y. Feng, *J. Nanopart Res.*,16 (2014) 2246.
26. Youkui Zhang,Wenkun Zhu,Xudong Cui,Weitang Yao and Tao Duan, *Cryst. Eng. Comm.*, 17 (2015) 8368.
27. Ye Cong, Jinlong Zhang, Feng Chen,MasakazuAnpo, and Dannong He, *J. Phys.Chem. C*, 111 (2007) 10618.
28. G.Wang, H. Wang, Y. Ling, Y. Tang, X. Yang, R.C. Fitzmorris, C.Wang, J.Z. Zhang, Y.Li, *Nano Lett.* 11 (2011) 3026.
29. C. Wang, Z Chen, H. Jin, C. Cao, J. Li and Z. Mi, *J. Mater. Chem. A,* 2 (2014)17820.
30. A. B. Lavand, Y. S. Malghe, *J Therm Anal Calorim* 123 (2016) 1163.